

Optical conductivity of URu₂Si₂ in the Kondo liquid and hidden-order phases

R. P. S. M. Lobo*

*ESPCI ParisTech, PSL Research University; CNRS; Sorbonne Universités, UPMC University of Paris 6, LPEM, 10 rue Vauquelin, F-75231 Paris Cedex 5, France*J. Buhot[†] and M. A. Méasson*Laboratoire Matériaux et Phénomènes Quantiques, UMR 7162 CNRS, Université Paris Diderot, Bât. Condorcet, 75205 Paris Cedex 13, France*

D. Aoki and G. Lapertot

*Université Grenoble Alpes, INAC-SPSMS, F-38000 Grenoble, France
and CEA, INAC-SX, F-38000 Grenoble, France*

P. Lejay

*CNRS, Institut Néel, F-38042 Grenoble, France
and Université Grenoble Alpes, Institut Néel, F-38042 Grenoble, France*

C. C. Homes

Condensed Matter Physics and Materials Science Department, Brookhaven National Laboratory, Upton, New York 11973, USA

(Received 17 June 2015; revised manuscript received 10 July 2015; published 29 July 2015)

We measured the polarized optical conductivity of URu₂Si₂ from room temperature down to 5 K, covering the Kondo state, the coherent Kondo liquid regime, and the hidden-order phase. The normal state is characterized by an anisotropic behavior between the *ab* plane and *c*-axis responses. The *ab*-plane optical conductivity is strongly influenced by the formation of the coherent Kondo liquid: a sharp Drude peak develops and a hybridization gap at 12 meV leads to a spectral weight transfer to mid-infrared energies. The *c*-axis conductivity has a different behavior: the Drude peak already exists at 300 K and no particular anomaly or gap signature appears in the coherent Kondo liquid regime. When entering the hidden-order state, both polarizations see a dramatic decrease in the Drude spectral weight and scattering rate, compatible with a loss of about 50% of the carriers at the Fermi level. At the same time a density-wave-like gap appears along both polarizations at about 6.5 meV at 5 K. This gap closes respecting a mean-field thermal evolution in the *ab* plane. Along the *c* axis it remains roughly constant and it “fills up” rather than closing.

DOI: [10.1103/PhysRevB.92.045129](https://doi.org/10.1103/PhysRevB.92.045129)

PACS number(s): 71.27.+a, 75.30.Mb, 78.30.-j

I. INTRODUCTION

A consequence of the open *5f* shells of uranium is an array of electronic properties with the same energy scale. Competition and cooperation among these properties in intermetallic URu₂Si₂, in particular between itinerant and localized *f* electrons, lead to a rich phase diagram [1–5]. URu₂Si₂ is a heavy fermion material with a Kondo temperature of 370 K [6]. At lower temperatures, hybridization between heavy *f* electrons with conduction electrons creates a crossover to a Kondo liquid state [7,8] having coherent transport properties below $T_{KL} \approx 70$ K. Upon further cooling, a second-order mean-field transition at $T_{HO} = 17.5$ K creates an electronically ordered state. The real nature of the order parameter remains unknown with the most varied hypothesis proposed [9–20]. Waiting for its elucidation the “hidden-order” moniker has been adopted to describe this phase [1]. Closing the series of thermal phase transitions, an unconventional superconducting phase appears below $T_c \approx 1.5$ K [21].

The hidden-order transition is associated with a partial gap opening in both spin and charge channels [6,22–26]. Recently, Shubnikov–de Hass [27–29], scanning tunnel microscopy (STM) [30,31], and angle-resolved photoemission spectroscopy (ARPES) [32–37] showed that URu₂Si₂ has a complex Fermi surface with a strong renormalization below T_{HO} . Point-contact spectroscopy [38–41], ultrafast pump-probe measurements [42], and optical conductivity [43] indicated the existence of a (pseudo)gap at temperatures ranging 19–30 K. In the case of point-contact spectroscopy, it was suggested that the effect could be related to a local increase in T_{HO} due to the pressure utilized to apply the contacts to the surface.

The unit cell of URu₂Si₂ has a tetragonal symmetry with space group $I4/mmm (D_{4h}^{17})$ [21] that seems to remain unchanged throughout the several phase transitions and transformations as a function of temperature, although this issue is still controversial [44,45]. In a tetragonal structure, the optical properties are fully defined by two different tensor elements. Measurements with the electric field of light $E \parallel a$ probe the *ab* tetragonal basal plane. When $E \parallel c$, the measurements reveal the *c*-axis properties.

The early optical conductivity measurements of URu₂Si₂ [22,46] assumed an antiferromagnetic (AFM) transition below T_{HO} . Even if the nature of the transition has

*lobo@espci.fr

[†]Present address: High Field Magnet Laboratory, Institute for Molecules and Materials, Radboud University Nijmegen, Toernooiveld 7, 6525 ED Nijmegen, The Netherlands.

since became unknown, their findings were not strictly tied to an AFM picture and fit nicely into the quest to understand the hidden-order character. Bonn *et al.* [22] were the first to measure the $E \parallel a$ electrodynamics of URu₂Si₂ and found a peak in the optical conductivity in the hidden-order phase, which had the properties of an optical gap that partially limited the states at the Fermi surface. Later, Degiorgi *et al.* [46] published a comprehensive set of $E \parallel a$ optical conductivity data on URu₂Si₂ in the framework of several other heavy fermion compounds. They observed the development of a Drude peak below T_{KL} , a clear far-infrared signature below T_{HO} , and estimated a mass enhancement of 68 at low temperatures, although this number is larger than what was previously proposed [5,30,47].

The last few years have seen the revival of the interest in the optical conductivity of URu₂Si₂. Levallois *et al.* [43] started this new wave and were also the first to measure the electrodynamics for $E \parallel c$. They essentially analyzed the response above T_{HO} and found a suppression of spectral weight around 12 meV, below 30 K, in both a and c responses. They assigned this effect to a possible Fermi-surface reconstruction crossover. Guo *et al.* [48] measured the ab plane reflectivity and concluded that the pseudogap observed in Ref. [43] was not a precursor of the hidden-order gap. Hall *et al.* [49] produced the first measurements along the c axis in the hidden-order phase. Interestingly they found two gaps along the c direction: one similar to its a counterpart and another of smaller energy and magnitude. A gap at the same energy was also observed in the A_{2g} symmetry by Raman spectroscopy [24,26].

Nagel *et al.* [47] showed that, just above T_{HO} but still at low enough temperatures, the in-plane resistivity of URu₂Si₂ had a quadratic dependence in both temperature (T) and frequency (ω). They also showed that this property is not a sufficient condition to characterize a Fermi liquid as the ratio between the multiplying factors in T and ω did not respect Landau's predictions.

In this paper we show the polarized optical conductivity of URu₂Si₂ from room temperature through the Kondo liquid state and into the hidden-order phase. In Sec. II we describe our samples and apparatus. Section III describes qualitatively our measured reflectivity and optical conductivity. We discuss the Kondo liquid state in Sec. IV, where we find a $E \parallel a$ optical response strongly dependent on the Kondo physics with the formation of a coherent Drude peak and the opening of a hybridization gap at 12 meV below T_{KL} . Conversely, the $E \parallel c$ data do not show any particular anomaly at T_{KL} and no signature of a hybridization gap. Section V analyzes our results in the hidden-order phase. The strong band-structure renormalization leads to a significant decrease of the Drude spectral weight as well as a large drop in the quasiparticle scattering rate. Both polarizations show the opening of a density-wave-like gap at about 6.5 meV. The gap closes with a mean-field behavior along $E \parallel a$. For the $E \parallel c$ direction it fills up when approaching T_{HO} with little temperature dependence. Our conclusions are summarized in Sec. VI.

II. METHODS

Two single crystals were utilized in this study. The first crystal (sample A) was grown in a tri-arc furnace under argon

atmosphere with a subsequent annealing under UHV at 900 °C for 10 days. It had a surface containing the ab plane of about 3×6 mm² and it was about 200 μ m thick. The second crystal (sample B) was grown by the Czochralski method using a tetra-arc furnace [50]. This sample was polished with a surface of 1×1.5 mm² containing the ac plane. It was further annealed under UHV at 950 °C for two days in order to release the mechanical damage introduced by polishing [51].

We utilized three different spectrometers to measure the near-normal incidence reflectivity from the far-infrared to the deep-UV: (i) a Bruker IFS113v from 2 meV (15 cm⁻¹) to 12 meV (100 cm⁻¹); (ii) a Bruker IFS66v from 6 meV (50 cm⁻¹) to 2 eV (15 000 cm⁻¹); and (iii) an AvaSpec 2048 \times 14 optical fiber spectrometer from 1.5 eV (12 000 cm⁻¹) to 5 eV (40 000 cm⁻¹). We obtained the absolute value of the reflectivity with an *in situ* gold evaporation technique [52]. Our absolute accuracy is 0.5% and the relative accuracy between different temperatures is better than 0.1%. The spectral resolution was 2 cm⁻¹ (0.25 meV) in both Bruker spectrometers and 2 nm for the visible and UV ranges.

Measurements on sample A were taken on freshly cleaved surfaces and were restricted to the $E \parallel a$ geometry. We did not use optical polarizers for this data set and we collected spectra at several temperatures from 5 to 300 K from 2 meV (15 cm⁻¹) to 2 eV (15 000 cm⁻¹). We extended this data to 5 eV (40 000 cm⁻¹) at room temperature only.

We utilized holographic wire grid polarizers on polyethylene and KRS-5 substrates to determine the $E \parallel c$ response on sample B at several temperatures on a spectral range from 2 meV (15 cm⁻¹) to 1 eV (8 000 cm⁻¹). We also measured the $E \parallel a$ polarization for this sample at 5, 50, and 300 K in the far infrared. We found the same results as the ones obtained in cleaved sample A.

Other optical functions were obtained from Kramers-Kronig analysis. At low energies we utilized a $1 - R \propto \sqrt{\omega}$ Hagen-Rubens extrapolation. For energies higher than our last temperature-dependent point, we built a spectrum in four steps: (i) the $E \parallel a$ 300-K data up to 5 eV (40 000 cm⁻¹); (ii) Degiorgi *et al.* [46] data up to 12.5 eV (100 000 cm⁻¹); (iii) x-ray cross-section reflectivity [53] up to 125 eV (1 000 000); and (iv) a free-electron ω^{-4} termination. We utilized this spectrum, at all temperatures, as the extension for the $E \parallel a$ above 2 eV and, properly normalized, for $E \parallel c$.

III. RESULTS

Figure 1 shows the far-infrared reflectivity for both polarizations as a function of temperature. Panel (a) shows the $E \parallel a$ response with a metallic profile at all temperatures. The sharp peaks at 15 and 45 meV are the two expected E_u phonons [25]. The reflectivity increases steadily upon cooling the sample down to ~ 75 K. For lower temperatures, the reflectivity decreases below 45 meV and then increases again below 15 meV. In the hidden-order phase, a strong dip appears in the reflectance around 5 meV. The detailed temperature evolution of this hidden-order signature is depicted in panel (c). Note that its leading edge is constant but its trailing edge and amplitude are both strongly temperature dependent.

Figure 1(b) shows the $E \parallel c$ reflectivity. When compared to the $E \parallel a$ response, we note a few distinctions. Phonon

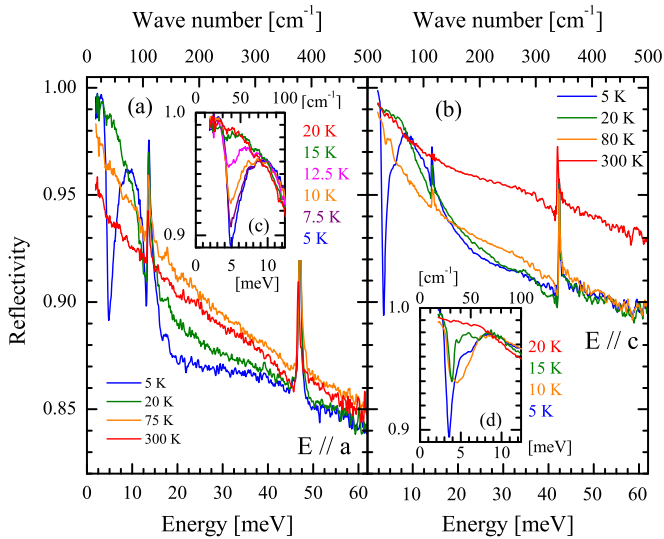


FIG. 1. (Color online) Reflectivity of URu₂Si₂ above and below the hidden-order transition for (a) $E \parallel a$ and (b) $E \parallel c$ polarizations. Panels (c) and (d) detail the very far-infrared reflectivity in the hidden-order phase for both polarizations.

frequencies are slightly different as they correspond to the two expected modes for the one-dimensional A_{2u} representation [25]. The low-energy increase in the reflectivity is not as conspicuous. There is no clear temperature or energy marking a reflectivity decrease, we rather see a continuous evolution from 300 K. A similar hidden-order dip appears below T_{HO} . However, as detailed in panel (d), its temperature evolution is quite different.

Figure 2 shows the Kramers-Kronig obtained real part of the optical conductivity (σ_1). The sharp peaks around 15 and 45 meV are polar phonons and have been discussed extensively by Buhot *et al.* [25]. Panel (a) shows σ_1 for $E \parallel a$. At 300 K, URu₂Si₂ has an incoherent conductivity along a without a clear Drude-like peak. In quite an opposite behavior, σ_1 actually shows a slight downturn at low frequencies. When cooling the material, one can discern a hint of a Drude peak at 150 K, which becomes well established upon further cooling down to 25 K. Below the hidden-order transition temperature, this Drude term collapses and a strong peak appears around 8 meV. This peak is directly related to the dip observed in the reflectivity.

Figure 2(b) shows σ_1 for $E \parallel c$. Contrary to the ab -plane response, a Drude-like peak is already present at room temperature. The absolute value of the optical conductivity is roughly three times larger when compared to $E \parallel a$ values, in accordance with the smaller dc resistivity. Upon cooling the sample, the optical conductivity below 40 meV decreases continuously, qualitatively suggesting a Drude peak narrowing at low temperatures, as we will discuss in Sec. IV. Once again, the hidden-order transition marks the appearance of a strong far-infrared peak with a significant redistribution of local spectral weight.

IV. KONDO LIQUID STATE

Let us first concentrate on the optical properties of URu₂Si₂ at temperatures above the hidden-order transition. Besides the

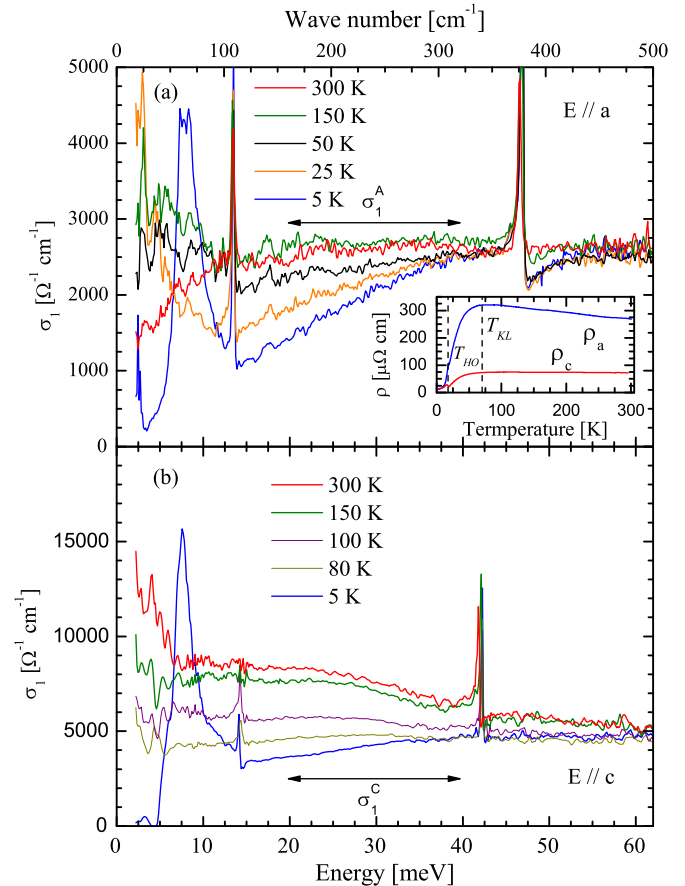


FIG. 2. (Color online) Optical conductivity of URu₂Si₂ for (a) $E \parallel a$ and (b) $E \parallel c$. The $E \parallel c$ dc limit of σ_1 is roughly three times higher than its value for $E \parallel a$ (note the difference in the optical conductivity scale), in accordance with the strongly anisotropic transport behavior of URu₂Si₂. In the 20–40-meV range we observe a decrease of spectral weight related to a narrowing of the Drude peak. For $E \parallel a$ this effect happens mostly below the Kondo temperature. For $E \parallel c$ the spectral weight decreases continuously from room temperature. Below the hidden order a strong peak appears at roughly 8 eV with a strong decrease of σ_1 at lower energies, characteristic of a partial gap at the Fermi level. The inset shows the resistivity from Refs. [4,47,54] (see text). The vertical dashed lines indicate the hidden-order transition and the boundary of the coherent Kondo liquid regime.

hidden-order signature, Fig. 2 shows large changes in the optical conductivity below ~ 40 meV. To discuss this effect and avoid complications due to phonons and the hidden-order feature, we will concentrate our analysis in the 20–40-meV region. We define σ_1^{Ia} and σ_1^{Ic} as the optical conductivity in this intermediate region for $E \parallel a$ and $E \parallel c$, respectively.

σ_1^{Ia} remains almost temperature independent from 300 K down to about 75 K, roughly T_{KL} . Below this temperature, it decreases significantly whereas the low-energy conductivity increases with the development of a Drude peak. Conversely, along the c axis the optical conductivity shows a far-infrared Drude-like peak at all temperatures and σ_1^{Ic} decreases steadily from 300 K.

The inset of Fig. 2(a) shows the resistivity of URu₂Si₂. Data for ρ_a were measured for a specimen from the same batch as our sample A and is extracted from Ref. [47]. The low-temperature ($T < 25$ K) c -axis resistivity is from Ref. [54]. It was extended to higher temperatures with a proper renormalization of the data in Ref. [4].

We can qualitatively explain the optical conductivity behavior from the temperature dependence of the resistivity. As ρ_c is smaller than ρ_a it is reasonable to find a room-temperature Drude peak in the former and not the latter. A temperature decrease leads to a slight increase in ρ_a down to the coherent Kondo liquid temperature, explaining why $\sigma_1^{I_a}$ remains roughly constant down to T_{KL} . The dramatic drop in ρ_a below T_{KL} is accompanied by the formation of a Drude peak in the $E \parallel a$ polarization. The narrowing of this Drude peak leads to the observed decrease in $\sigma_1^{I_a}$. Along the c axis, the relative decrease in ρ_c is not as strong as the one observed along a . The steady decrease in $\sigma_1^{I_c}$ can again be understood as a continuous Drude narrowing.

In heavy fermion compounds the Drude response is strongly renormalized by the effective mass [55], producing very narrow peaks [46,56,57], difficult to access from the optical conductivity. For example, the low-temperature scattering rate in UPd₂Al₃ is about 3 GHz (0.012 meV or 0.1 cm⁻¹), a value more than two orders of magnitude smaller than our lowest measured frequency. The mass enhancement in URu₂Si₂ is smaller but comparable to that in UPd₂Al₃ [57] and one should also expect a narrow Drude peak. Indeed, $\rho_a^{-1}(T = 5 \text{ K}) \approx 70\,000 \text{ } \Omega^{-1} \text{ cm}^{-1}$, an order of magnitude larger than the scale shown in Fig. 2(a). This can only be explained by a very narrow Drude peak with a scattering rate much smaller than the lowest measured energy. Such narrow peaks are more easily seen in the frequency-dependent dielectric function, which can be parametrized by

$$\varepsilon(\omega) = \varepsilon_{el} + \varepsilon_{ph} + \varepsilon_{HO} - \frac{\Omega_p^2}{\omega^2 + i\omega/\tau}, \quad (1)$$

where the first three terms on the right-hand side are contributions from electronic transitions (ε_{el}), phonons (ε_{ph}), and the hidden order (ε_{HO}). The last term is the Drude response from free carriers, characterized by a plasma frequency (Ω_p) and a scattering rate ($1/\tau$). We note that, when $1/\tau$ is small when compared to the lowest measured frequency, the real part of the dielectric function— $\varepsilon_1(\omega)$ —has a negative ω^{-2} divergence. The Drude model is a very crude single band approximation for mobile carriers in strongly correlated systems as it takes into account neither a frequency-dependent scattering rate [58,59] nor multiband effects. However, it is a very good approximation for the low-frequency response [60].

Figure 3 shows $\varepsilon_1(\omega)$ for both polarizations. Panel (a) shows a low-energy positive upturn in ε_1 at 200 K for $E \parallel a$. This means that no coherent, well established Drude peak exists for this temperature. This situation persists down to temperatures close to T_{KL} . Only at 75 K (not shown) could we detect a slight hint of a negative low frequency $\varepsilon_1(\omega)$. This Drude signature gets stronger from T_{KL} down to T_{HO} and remains present in the hidden-order phase. This means that, in agreement with the decreasing resistivity, the opening of a gap below T_{HO} does not

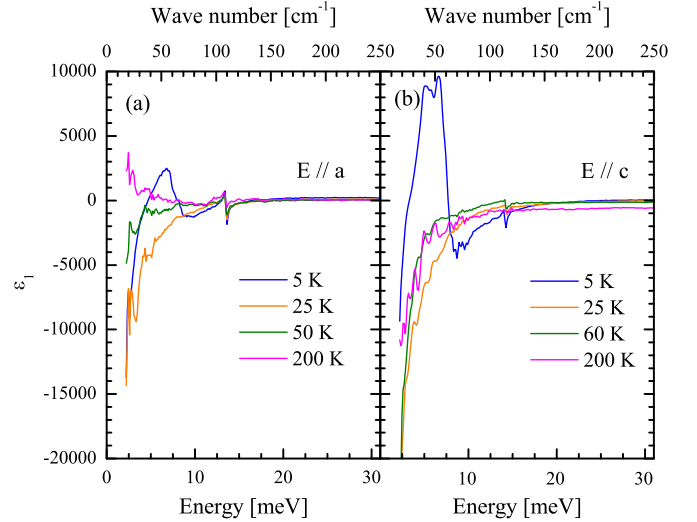


FIG. 3. (Color online) Real part of the dielectric function for (a) $E \parallel a$ and (b) $E \parallel c$. At very low energies a negative divergence, due to the Drude contribution to Eq. (1), dominates the spectral response and allows us to determine the plasma frequency and scattering rate. The peaks around 15 meV correspond to polar phonons. In the hidden-order state another large peak appears around 5 meV. Note that a well defined negative divergence is present at all temperatures for $E \parallel c$ but only below 75 K for $E \parallel a$.

happen over the full Fermi surfaces, i.e., this is a partial gap. Panel (b) shows $\varepsilon_1(\omega)$ for $E \parallel c$. The remarkable difference with respect to the a direction is that the Drude signature is present at all temperatures and not only below T_{KL} .

The presence of a Drude signature at low temperatures validates our picture of a very narrow Drude peak in σ_1 at low temperatures. The last term in Eq. (1) allows us to estimate the plasma frequency and the scattering rate of this narrow Drude component. The Drude parameters for both polarizations are shown in Fig. 4. We will discuss the hidden-order phase in Sec. V. Here we concentrate on the normal state.

As we mentioned before, in the $E \parallel a$ polarization the Drude term only exists below T_{KL} . From that temperature down to T_{HO} the plasma frequency is constant. No sign of a normal-state gap opening or band renormalization is present. The scattering rate decreases monotonically as for a regular metal. The $E \parallel c$ polarization also shows a constant normal-state plasma frequency and, for this orientation, no effect of the Kondo transition is visible. Its scattering rate also decreases monotonically with temperature.

As the low-energy Drude peak is not well defined at all temperatures (in particular for $E \parallel a$), we can attempt to infer the free carrier behavior from the optical conductivity in the intermediate regions $\sigma_1^{I_a}$ and $\sigma_1^{I_c}$. For that, we define a restricted spectral weight, which measures the local charge distribution:

$$S(\omega_0, \omega_1) = \int_{\omega_0}^{\omega_1} \sigma_1(\omega) d\omega. \quad (2)$$

When $\omega_0 \rightarrow 0$ and $\omega_1 \rightarrow \infty$, Eq. (2) yields $S = (\pi/2)\varepsilon_0\Omega_p^2$ leading to the standard f -sum rule.

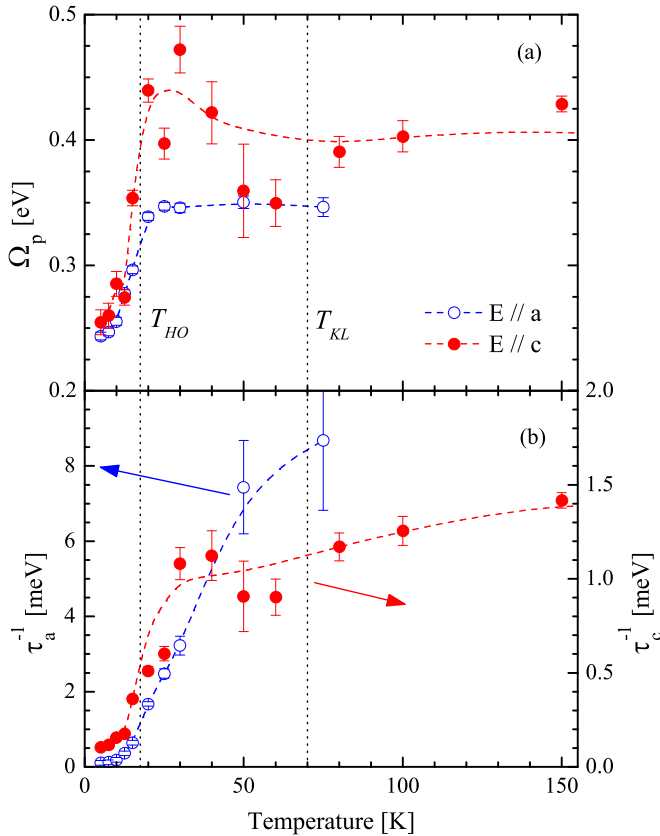


FIG. 4. (Color online) Drude parameters extracted from the low-energy real part of the dielectric function (Fig. 3). Panel (a) shows the plasma frequency and panel (b) the scattering rate. There is no well defined Drude peak above ~ 100 K for data with $E \parallel a$. The vertical dotted lines indicate the position of T_{HO} and T_{KL} . The dashed lines are guides to the eye. For clarity the data are only shown up to 150 K along $E \parallel c$. Above that temperature Ω_p is roughly constant and $1/\tau$ increases slightly. Error bars are estimated by utilizing different models for the hidden-order and phonon excitations as well as by varying the spectral range allowed for a least-squares fitting of the Drude term.

We obtain Fig. 5 by setting $\omega_0 = 20$ meV (160 cm^{-1}) and $\omega_1 = 40$ meV (320 cm^{-1}), normalized by 300-K values. Along the a direction we see that the total spectral weight in the intermediate region is roughly constant down to the Kondo liquid coherence temperature. This is a consequence of an almost incoherent transport as shown by the absence of a low-energy peak in the data. At T_{KL} the coherent far-infrared Drude peak appears. The integrated $\sigma_1^{I_a}$ steadily decreases, indicating, as a first approximation, the narrowing of the Drude peak. This behavior corroborates the parameters found in Fig. 4 and indicates that the $E \parallel a$ electrodynamic in the normal state is dominated by the Kondo physics.

The Drude parameters already hinted to us that the $E \parallel c$ polarization was not strongly influenced by the coherent Kondo liquid formation. Figure 5 confirms this observation by showing a continuous decrease of the total spectral weight in the intermediate region, with no features at T_{KL} . This decrease is compatible with the observed steady decrease, from room temperature, of $1/\tau_c$ and a constant Ω_p .

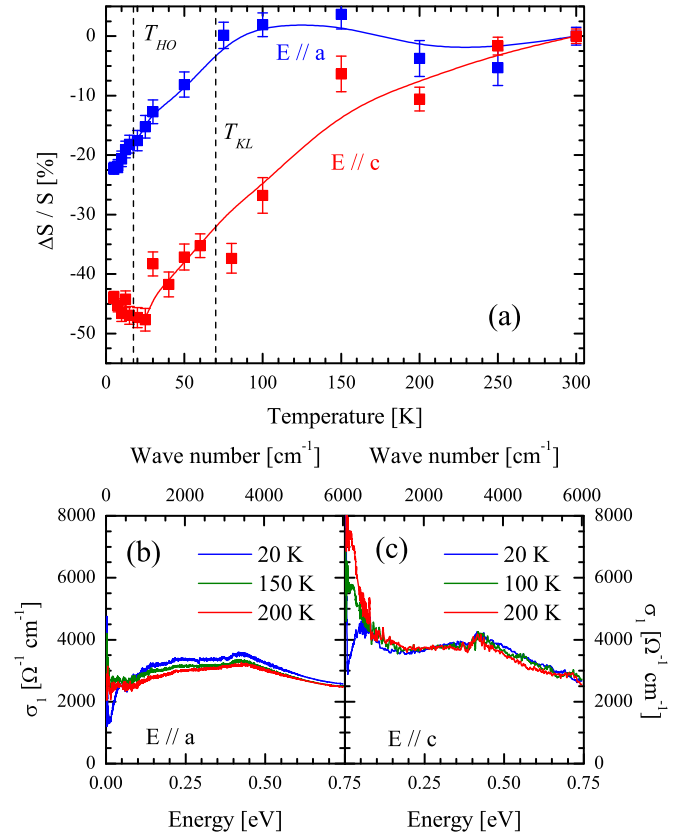


FIG. 5. (Color online) (a) Restricted spectral weight, normalized to its value at 300 K, calculated with $\omega_0 = 20$ meV (160 cm^{-1}) and $\omega_1 = 40$ meV (320 cm^{-1}). The solid lines are guides to the eye. The vertical dashed lines indicate the hidden-order transition and the boundary of the coherent Kondo liquid regime. Error bars are obtained by varying the cutoff frequencies by $\pm 10\%$. Optical conductivity for (b) $E \parallel a$ and (c) $E \parallel c$ in the midinfrared range. Phonons were subtracted for clarity. For $E \parallel a$, part of the spectral weight lost in the 20–40-meV range (see Fig. 2) is transferred to the 0.5-eV region, indicating the opening of a gap above T_{HO} . Along $E \parallel c$ no such transfer is observed, within the accuracy of our data.

It is important to note that the decrease in $\sigma_1^{I_a}$ cannot be solely associated to the narrowing of the Drude peak. The decrease in the $\sigma_1^{I_a}$ spectral weight below T_{KL} is not fully recovered in the Drude peak as extracted from $\epsilon_1(\omega)$. Some of this spectral weight is transferred to the 0.5-eV region [48]. This indicates that some of the spectral weight lost here is due to the hybridization gap opening. However, contrary to Refs. [43,48] we observe this gap opening in the vicinity of T_{KL} rather than 30 K. Note that Fig. 2(a) shows this gap undoubtedly present at 50 K.

We can see further support for a gaplike structure related to the spectral weight decrease in $\sigma_1^{I_a}$ by looking at its evolution in the hidden-order phase. The small scattering rate in the hidden-order phase, as shown in Fig. 4, suggests that one should not expect any Drude spectral weight in the intermediate region used to calculate ΔS of Fig. 5. The fact that this spectral weight continues to decrease in the hidden-order phase means that it is being transferred not to the Drude peak but to higher energies. This also corroborates

the view of independent hybridization and hidden-order gaps. Further evidence for a gap in the normal state for $E \parallel a$ can be inferred from Fig. 5(b). It shows an increase in the midinfrared (around 0.5 eV) concomitant with the decrease observed in the 20–40-meV region (Fig. 2), indicating that a transfer from low to high energies is also present, besides the narrowing of the Drude peak. The determination of the exact gap energy from the optical conductivity is model dependent. Nevertheless, gap values can be inferred by minima or by inflection points in $\sigma_1(\omega)$. Figure 2(a) shows that σ_1 at $T = 25$ K has a minimum around 12 meV. This is the same energy observed in optics [43,48] and by other techniques [5,35,36].

Conversely, along $E \parallel c$, we observe a saturation of ΔS in the hidden-order phase, when $1/\tau_c$ collapses. There is no sign of spectral weight transfer to higher frequencies, suggesting the absence of a hybridization gap in this direction. Indeed, inspection of Fig. 2(b) does not reveal any clear minimum in σ_1 for $E \parallel c$ in the normal state, which could be associated to a gap energy. Figure 5(c) further supports the absence of a hybridization gap signature along $E \parallel c$. Within the accuracy of our data, we observe no changes in the midinfrared $E \parallel c$ conductivity when going through the Kondo liquid coherence temperature. There is no midinfrared spectral weight gain associated to the decrease in the 20–40-meV range.

We can summarize our findings for the optical conductivity of URu₂Si₂ above T_{HO} as (i) the Kondo coherence response is anisotropic; (ii) the $E \parallel a$ electrodynamic is strongly dominated by Kondo physics with the formation of a very sharp Drude peak below T_{KL} ; (iii) the narrowing of the Drude peak does not account for all the spectral weight lost in the 30-meV region and part of it is due to the hybridization gap that opens below T_{KL} at ~ 12 meV; (iv) this hybridization gap is observed along the $E \parallel a$ polarization but not along $E \parallel c$; (v) the decrease in σ_1 in the 20–40-meV region for $E \parallel c$ is fully attributable to a narrowing of a Drude peak, which starts at room temperature; (vi) we observed no influence of the coherent Kondo liquid formation in the $E \parallel c$ optical conductivity; (vii) in contrast to Ref. [43], we did not observe any effect related to a possible pseudogap opening at 30 K.

V. HIDDEN ORDER

When entering the hidden-order state, a sharp dip appears in the reflectivity, which leads to a peak in the far-infrared optical conductivity, as shown in Fig. 6. The overall behavior for both polarizations is the same. A Drude-like peak dominates σ_1 just above T_{HO} . In the hidden-order phase, a large peak appears around 8 meV at the expense of a strong depletion in the low-energy σ_1 . It is worth noting that in both cases, the spectral weight below 20 meV is conserved between the normal and the hidden-order state, i.e., the lost σ_1 at low energies corresponds to the area gained by the 8-meV peak. This “low-to-high” spectral weight transfer is a textbook example of a density wave gap (see Chaps. 7 and 14 of Ref. [61]).

One should take the “density wave” terminology with caution. It simply means that the transfer of spectral weight is from below to above the gap energy, as opposed to a superconducting gap (transfer from finite energies to dc) or a semiconducting gap (gap developed over the whole Fermi

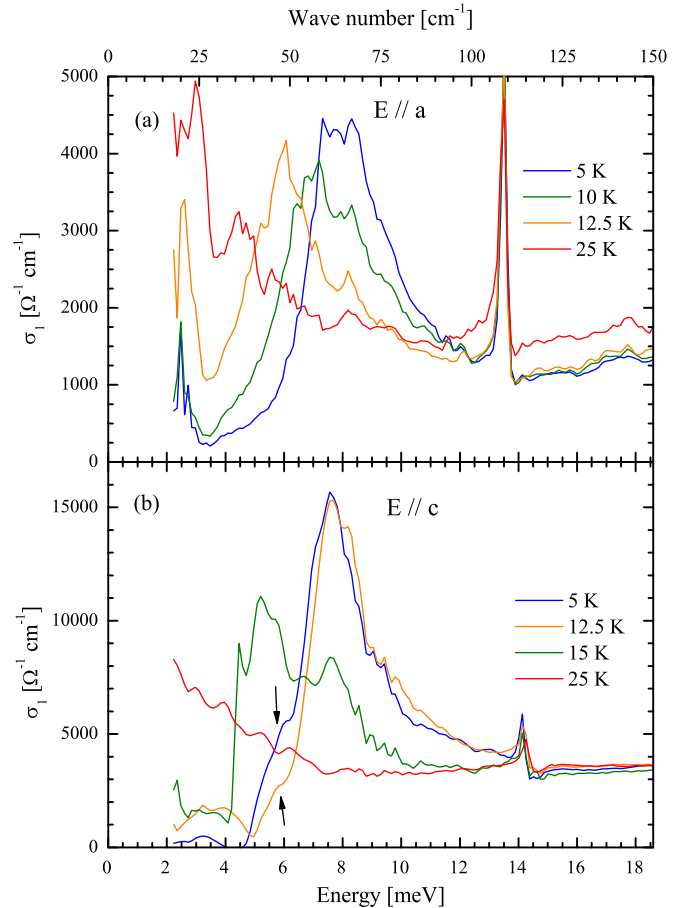


FIG. 6. (Color online) Real part of the optical conductivity in the hidden-order phase for (a) $E \parallel a$ and (b) $E \parallel c$. The large peak around 8 meV indicates the opening of a gap. In both cases, we can estimate (from the inflexion point) a gap $2\Delta_{HO} \approx 6.5$ meV at 5 K. The opening of the gap transfers spectral weight from low (just below $2\Delta_{HO}$) to high (just above $2\Delta_{HO}$) energies. Note that for $E \parallel a$ the gap closes, i.e., its energy continuously decreases upon increasing temperature. For $E \parallel c$ the gap fills up rather than closes. Also note a small shoulder (indicated by the arrows) at the leading edge of the hidden-order peak along c , showing the presence of a second gap in this orientation. In both panels, the sharp peaks around 14 meV are polar phonons.

surface with strictly zero absorption up to the gap energy). The gap behavior in URu₂Si₂ does not mean that the hidden order is a density wave transition. However, it does impose that any model for the hidden-order transition must account for a gap with a spectral weight redistribution similar to that of a density-wave instability.

The opening of a hidden-order gap comes from the strong band-structure renormalization observed below T_{HO} [35,36]. However, in both polarizations, this gap is only partial. Indeed, the resistivity (inset of Fig. 2) shows an increasing metallic character in the hidden-order state corresponding to the survival of a Drude peak in the dielectric function (Fig. 3) down to our lowest measured temperature. Figure 4(a) shows that the plasma frequency decreases dramatically at T_{HO} , but does not vanish completely. The plasma frequency is related to microscopic quantities through $\Omega_p^2 = ne^2/\epsilon_0 m$. We can

estimate the mobile charge density lost in the hidden-order state from the ratio $[\Omega_p^{(4K)}/\Omega_p^{(25K)}]^2$. We find that 50% of the mobile carriers are lost in the $E \parallel a$ direction and 60% along c . This is in agreement with early results that estimated a partial gap opening over about 40% of the Fermi surface [5,21].

A closer analysis of the hidden-order gap shows remarkable differences between a and c responses. Figure 6(a) shows the $E \parallel a$ spectra. Defining the exact gap energy is model dependent. A safe approach is to take the inflection point in the leading edge of the peak as a first (slightly overestimated) approximation of $2\Delta_{HO}$, the energy necessary to excite a charge from the highest occupied state to the lowest empty state. From this perspective, panel (a) shows a hidden-order gap that decreases in both energy and spectral weight with the temperature, whereas panel (b) shows that the gap along the c axis keeps the same spectral weight and energy up to, at least, $0.7 T_{HO}$. In addition a small shoulder (indicated by the arrows) appears at the leading edge of the $E \parallel c$ gap. This is the signature of a second gap along that direction as observed by Hall *et al.* [49] and discussed in detail in that paper.

For the $E \parallel a$ data, the spectral weight redistributed by the hidden order decreases continuously from 5 K, suggesting that states at the Fermi level are recovered fast when approaching T_N . In the $E \parallel c$ polarization, the density of states lost at the Fermi level do not change until one gets close to T_{HO} . This observation can also be inferred from Fig. 4(a) where the value of the plasma frequency along c drops, in the hidden-order phase, at a faster pace than in the ab plane.

Figure 7 shows the temperature evolution of the hidden-order gap for both orientations. Along the $E \parallel a$ direction, the gap energy decreases with increasing temperature following a

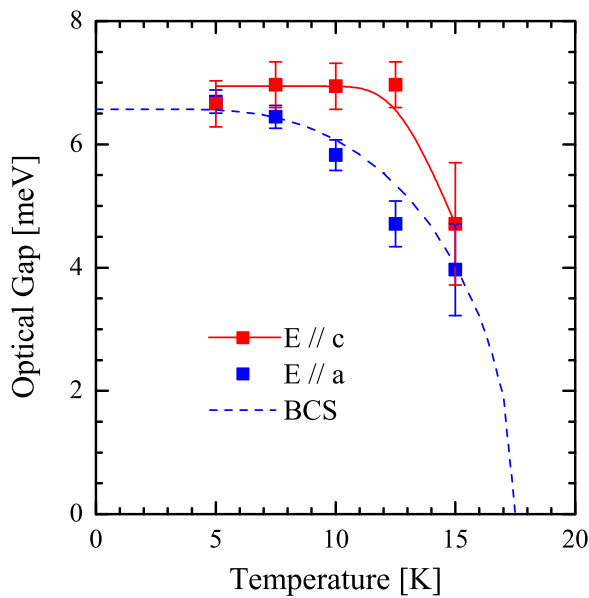


FIG. 7. (Color online) Temperature dependence of the hidden-order gap energy, taken as the inflection point of the leading edge of the peak in Fig. 6. Blue symbols correspond to the $E \parallel a$ optical conductivity and red symbols to the c axis. The dashed line is the result of a mean-field BCS calculation and the solid line is a guide to the eye.

mean-field BCS-like behavior. Looking at Fig. 6(a), one can also see that when the gap closes, the low-frequency optical conductivity increases, indicating the presence of thermally excited quasiparticles. The c -axis behavior is qualitatively very different. The gap energy stays fixed up to temperatures very close to T_{HO} . We do not find the quasi-mean-field behavior observed in Ref. [49]. It does not close but rather “fills up.” In addition, the gap remains robust with almost no creation of low-energy thermally excited quasiparticles almost all the way up to T_{HO} .

In the hidden-order phase a summary of our findings are as follows: (i) passing the hidden-order transition leads to the opening of a density-wave-like gap with spectral weight transfer from just below to just above the gap energy; (ii) the gap value is isotropic at 5 K but (iii) its thermal evolution is very different between $E \parallel a$ and $E \parallel c$; (iv) the temperature evolution of the gap energy along $E \parallel a$ follows a BCS mean-field behavior but (v) in the $E \parallel c$ polarization it stays constant almost all the way up to T_{HO} ; (vi) the $E \parallel a$ gap closes when approaching T_{HO} while the $E \parallel c$ gap fills up with almost no creation of thermally excited quasiparticles; (vii) we confirm the Hall *et al.* [49] observation of a second gap along the c direction.

VI. CONCLUSIONS

We measured the optical conductivity of URu₂Si₂ in the normal and hidden-order state with $E \parallel a$ and $E \parallel c$ polarizations. Our results show strong anisotropic behaviors at all temperatures. In the normal state, we found an anisotropic behavior with respect to the Kondo liquid coherence formation. Along $E \parallel a$ an incoherent optical conductivity is present down to T_{KL} where a sharp Drude peak develops. Conversely, along $E \parallel c$ this Drude peak is already present at room temperature and shows no particular anomaly at T_{KL} . We observed the opening of a gap, due to the hybridization of localized f electrons with mobile carriers, at temperatures very close to T_{KL} . It appears at an energy of 12 meV along the $E \parallel a$ direction. We did not find a gap signature in the Kondo liquid state for $E \parallel c$. The Drude spectral weight of both polarizations decreases dramatically when entering the hidden-order phase and we estimate a loss of about 50% of the carriers at the Fermi level. A fast drop in the scattering rate accompanies this decrease of spectral weight. A density-wave-like gap appears along both polarizations in the hidden-order state at about 6.5 meV at 5 K. Along $E \parallel a$ this gap closes following a mean-field thermal evolution. Along $E \parallel c$ the gap remains constant almost all the way up to T_{HO} and it fills up rather than closing.

ACKNOWLEDGMENTS

We thank D. B. Tanner, T. Timusk, G. Kotliar, A. Millis, and C. Pépin for fruitful discussions. Work at Brookhaven National Laboratory was supported by the Office of Science, U.S. Department of Energy, under Contract No. DE-SC0012704. The work in Université Paris Diderot was supported by the French Agence Nationale de la Recherche (ANR PRINCESS) and the Labex SEAM (Grant No. ANR-11-IDEX-0005-02).

- [1] J. A. Mydosh and P. M. Oppeneer, *Colloquium* : Hidden order, superconductivity, and magnetism: The unsolved case of URu₂Si₂, *Rev. Mod. Phys.* **83**, 1301 (2011).
- [2] J. A. Mydosh and P. M. Oppeneer, Hidden order behaviour in URu₂Si₂ (a critical review of the status of hidden order in 2014), *Philos. Mag.* **94**, 3642 (2014).
- [3] W. Schlabitz, J. Baumann, R. Pollit, U Rauchschalbe, H. M. Mayer, U. Ahlheim, and C. D. Bredl, Superconductivity and magnetic order in a strongly interacting Fermi-system: URu₂Si₂, *Z. Phys. B* **62**, 171 (1986).
- [4] T. T. M. Palstra, A. A. Menovsky, and J. A. Mydosh, Anisotropic electrical resistivity of the magnetic heavy-Fermion superconductor URu₂Si₂, *Phys. Rev. B* **33**, 6527 (1986).
- [5] M. B. Maple, J. W. Chen, Y. Dalichaouch, T. Kohara, C. Rossel, M. S. Torikachvili, M. W. McElfresh, and J. D. Thompson, Partially gapped Fermi surface in the heavy-electron superconductor URu₂Si₂, *Phys. Rev. Lett.* **56**, 185 (1986).
- [6] J. Schoenes, C. Schönenberger, J. J. M. Franse, and A. A. Menovsky, Hall-effect and resistivity study of the heavy-Fermion system URu₂Si₂, *Phys. Rev. B* **35**, 5375 (1987).
- [7] Y. F. Yang, Z. Fisk, H. O. Lee, J. D. Thompson, and D. Pines, Scaling the Kondo lattice, *Nature (London)* **454**, 611 (2008).
- [8] S. V. Dordevic, D. N. Basov, N. R. Dilley, E. D. Bauer, and M. B. Maple, Hybridization gap in heavy Fermion compounds, *Phys. Rev. Lett.* **86**, 684 (2001).
- [9] P. Santini and G. Amoretti, Crystal field model of the magnetic properties of URu₂Si₂, *Phys. Rev. Lett.* **73**, 1027 (1994).
- [10] Kristjan Haule and Gabriel Kotliar, Arrested Kondo effect and hidden order in URu₂Si₂, *Nat. Phys.* **5**, 796 (2009).
- [11] S. Elgazzar, J. Ruzs, M. Amft, P. M. Oppeneer, and J. A. Mydosh, Hidden order in URu₂Si₂ originates from Fermi surface gapping induced by dynamic symmetry breaking, *Nat. Mater.* **8**, 337 (2009).
- [12] C. Pépin, M. R. Norman, S. Burdin, and A. Ferraz, Modulated spin liquid: A new paradigm for URu₂Si₂, *Phys. Rev. Lett.* **106**, 106601 (2011).
- [13] H. Kusunose and H. Harima, On the hidden order in URu₂Si₂ – antiferro hexadecapole order and its consequences, *J. Phys. Soc. Jpn.* **80**, 084702 (2011).
- [14] E. Ressouche, R. Ballou, F. Bourdarot, D. Aoki, V. Simonet, M. T. Fernandez-Diaz, A. Stunault, and J. Flouquet, Hidden order in URu₂Si₂ unveiled, *Phys. Rev. Lett.* **109**, 067202 (2012).
- [15] H. Ikeda, M. T. Suzuki, R. Arita, T. Takimoto, T. Shibauchi, and Y. Matsuda, Emergent rank-5 nematic order in URu₂Si₂, *Nat. Phys.* **8**, 528 (2012).
- [16] J. G. Rau and H. Y. Kee, Hidden and antiferromagnetic order as a rank-5 superspin in URu₂Si₂, *Phys. Rev. B* **85**, 245112 (2012).
- [17] P. Chandra, P. Coleman, and R. Flint, Hastic order in the heavy-Fermion compound URu₂Si₂, *Nature (London)* **493**, 621 (2013).
- [18] C. Thomas, S. Burdin, C. Pépin, and A. Ferraz, Three-dimensional modulated spin liquid model applied to URu₂Si₂, *Phys. Rev. B* **87**, 014422 (2013).
- [19] T. Das, Imprints of spin-orbit density wave in the hidden-order state of URu₂Si₂, *Phys. Rev. B* **89**, 045135 (2014).
- [20] P. S. Riseborough, B. Coqblin, and S. G. Magalhães, Phase transition arising from the underscreened Anderson lattice model: A candidate concept for explaining hidden order in URu₂Si₂, *Phys. Rev. B* **85**, 165116 (2012).
- [21] T. T. M. Palstra, A. A. Menovsky, J. van den Berg, A. J. Dirkmaat, P. H. Kes, G. J. Nieuwenhuys, and J. A. Mydosh, Superconducting and magnetic transitions in the heavy-Fermion system URu₂Si₂, *Phys. Rev. Lett.* **55**, 2727 (1985).
- [22] D. A. Bonn, J. D. Garrett, and T. Timusk, Far-infrared properties of URu₂Si₂, *Phys. Rev. Lett.* **61**, 1305 (1988).
- [23] R. A. Fisher, S. Kim, Y. Wu, N. E. Phillips, M. W. McElfresh, M. S. Torikachvili, and M. B. Maple, Specific heat of URu₂Si₂: Effect of pressure and magnetic field on the magnetic and superconducting transitions, *Physica B* **163**, 419 (1990).
- [24] J. Buhot, M.-A. Méasson, Y. Gallais, M. Cazayous, A. Sacuto, G. Lapertot, and D. Aoki, Symmetry of the excitations in the hidden order state of URu₂Si₂, *Phys. Rev. Lett.* **113**, 266405 (2014).
- [25] J. Buhot, M. A. Méasson, Y. Gallais, M. Cazayous, A. Sacuto, F. Bourdarot, S. Raymond, G. Lapertot, D. Aoki, L. P. Regnault, A. Ivanov, P. Piekarz, K. Parlinski, D. Legut, C. C. Homes, P. Lejay, and R. P. S. M. Lobo, Lattice dynamics of the heavy-Fermion compound URu₂Si₂, *Phys. Rev. B* **91**, 035129 (2015).
- [26] H. H. Kung, R. E. Baumbach, E. D. Bauer, V. K. Thorsmolle, W. L. Zhang, K. Haule, J. A. Mydosh, and G. Blumberg, Chirality density wave of the hidden-order phase in URu₂Si₂, *Science* **347**, 1339 (2015).
- [27] H. Shishido, K. Hashimoto, T. Shibauchi, T. Sasaki, H. Oizumi, N. Kobayashi, T. Takamasu, K. Takehana, Y. Imanaka, T. D. Matsuda, Y. Haga, Y. Onuki, and Y. Matsuda, Possible phase transition deep inside the hidden order phase of ultraclean URu₂Si₂, *Phys. Rev. Lett.* **102**, 156403 (2009).
- [28] E. Hassinger, G. Knebel, T. D. Matsuda, D. Aoki, V. Taufour, and J. Flouquet, Similarity of the Fermi surface in the hidden order state and in the antiferromagnetic state of URu₂Si₂, *Phys. Rev. Lett.* **105**, 216409 (2010).
- [29] M. M. Altarawneh, N. Harrison, S. E. Sebastian, L. Balicas, P. H. Tobash, J. D. Thompson, F. Ronning, and E. D. Bauer, Sequential spin polarization of the Fermi surface pockets in URu₂Si₂ and its implications for the hidden order, *Phys. Rev. Lett.* **106**, 146403 (2011).
- [30] A. R. Schmidt, M. H. Hamidian, P. Wahl, F. Meier, A. V. Balatsky, J. D. Garrett, T. J. Williams, G. M. Luke, and J. C. Davis, Imaging the Fano lattice to hidden order transition in URu₂Si₂, *Nature (London)* **465**, 570 (2010).
- [31] P. Aynajian, E. H. da Silva Neto, C. V. Parker, Y. Huang, A. Pasupathy, J. Mydosh, and A. Yazdani, Visualizing the formation of the Kondo lattice and the hidden order in URu₂Si₂, *Proc. Natl. Acad. Sci. USA* **107**, 10383 (2010).
- [32] A. F. Santander-Syro, M. Klein, F. L. Boariu, A. Nuber, P. Lejay, and F. Reinert, Fermi-surface instability at the ‘hidden-order’ transition of URu₂Si₂, *Nat. Phys.* **5**, 637 (2009).
- [33] R. Yoshida, Y. Nakamura, M. Fukui, Y. Haga, E. Yamamoto, Y. Onuki, M. Okawa, S. Shin, M. Hirai, Y. Muraoka, and T. Yokoya, Signature of hidden order and evidence for periodicity modification in URu₂Si₂, *Phys. Rev. B* **82**, 205108 (2010).
- [34] I. Kawasaki, S. I. Fujimori, Y. Takeda, T. Okane, A. Yasui, Y. Saitoh, H. Yamagami, Y. Haga, E. Yamamoto, and Y. Onuki, Band structure and Fermi surface of URu₂Si₂ studied by soft x-ray angle-resolved photoemission spectroscopy, *Phys. Rev. B* **83**, 235121 (2011).

- [35] S. Chatterjee, J. Trinckauf, T. Hänke, D. E. Shai, J. W. Harter, T. J. Williams, G. M. Luke, K. M. Shen, and J. Geck, Formation of the coherent heavy Fermion liquid at the hidden order transition in URu₂Si₂, *Phys. Rev. Lett.* **110**, 186401 (2013).
- [36] F. L. Boariu, C. Bareille, H. Schwab, A. Nuber, P. Lejay, T. Durakiewicz, F. Reinert, and A. F. Santander-Syro, Momentum-resolved evolution of the Kondo lattice into hidden order in URu₂Si₂, *Phys. Rev. Lett.* **110**, 156404 (2013).
- [37] C. Bareille, F. L. Boariu, H. Schwab, P. Lejay, F. Reinert, and A. F. Santander-Syro, Momentum-resolved hidden-order gap reveals symmetry breaking and origin of entropy loss in URu₂Si₂, *Nat. Commun.* **5**, 4326 (2014).
- [38] K. Hasselbach, J. R. Kirtley, and P. Lejay, Point-contact spectroscopy of superconducting URu₂Si₂, *Phys. Rev. B* **46**, 5826 (1992).
- [39] R. Escudero, F. Morales, and P. Lejay, Temperature dependence of the antiferromagnetic state in URu₂Si₂ by point-contact spectroscopy, *Phys. Rev. B* **49**, 15271 (1994).
- [40] S. Thieme, P. Steiner, L. Degiorgi, P. Wachter, Y. Dalichaouch, and M. B. Maple, Itinerant antiferro- and ferro-magnetic instability in re-doped URu₂Si₂: Optical and point-contact spectroscopy results, *Europhys. Lett.* **32**, 367 (1995).
- [41] J. G. Rodrigo, F. Guinea, S. Vieira, and F. G. Aliev, Point-contact spectroscopy on URu₂Si₂, *Phys. Rev. B* **55**, 14318 (1997).
- [42] M. K. Liu, R. D. Averitt, T. Durakiewicz, P. H. Tobash, E. D. Bauer, S. A. Trugman, A. J. Taylor, and D. A. Yarotski, Evidence of a hidden-order pseudogap state in URu₂Si₂ using ultrafast optical spectroscopy, *Phys. Rev. B* **84**, 161101 (2011).
- [43] J. Levallois, F. Lévy-Bertrand, M. K. Tran, D. Stricker, J. A. Mydosh, Y.-K. Huang, and D. van der Marel, Hybridization gap and anisotropic far-infrared optical conductivity of URu₂Si₂, *Phys. Rev. B* **84**, 184420 (2011).
- [44] S. Tonegawa, S. Kasahara, T. Fukuda, K. Sugimoto, N. Yasuda, Y. Tsuruhara, D. Watanabe, Y. Mizukami, Y. Haga, T. D. Matsuda, E. Yamamoto, Y. Onuki, H. Ikeda, Y. Matsuda, and T. Shibauchi, Direct observation of lattice symmetry breaking at the hidden-order transition in URu₂Si₂, *Nat. Commun.* **5**, 4188 (2014).
- [45] C. Tabata, T. Inami, S. Michimura, M. Yokoyama, H. Hidaka, T. Yanagisawa, and H. Amitsuka, X-ray backscattering study of crystal lattice distortion in hidden order of URu₂Si₂, *Philos. Mag.* **94**, 3691 (2014).
- [46] L. Degiorgi, S. Thieme, H. R. Ott, M. Dressel, G. Grüner, Y. Dalichaouche, M. B. Maple, Z. Fisk, C. Geibel, and F. Steglich, The electrodynamic response of heavy-electron materials with magnetic phase transitions, *Z. Phys. B* **102**, 367 (1997).
- [47] U. Nagel, T. Uleksin, T. Rößm, R. P. S. M. Lobo, P. Lejay, C. C. Homes, J. S. Hall, A. W. Kinross, S. K. Purdy, T. Munsie, T. J. Williams, G. M. Luke, and T. Timusk, Optical spectroscopy shows that the normal state of URu₂Si₂ is an anomalous Fermi liquid, *Proc. Natl. Acad. Sci. USA* **109**, 19161 (2012).
- [48] W. T. Guo, Z. G. Chen, T. J. Williams, J. D. Garrett, G. M. Luke, and N. L. Wang, Hybridization gap versus hidden-order gap in URu₂Si₂ as revealed by optical spectroscopy, *Phys. Rev. B* **85**, 195105 (2012).
- [49] J. S. Hall, U. Nagel, T. Uleksin, T. Rößm, T. Williams, G. Luke, and T. Timusk, Observation of multiple-gap structure in hidden order state of URu₂Si₂ from optical conductivity, *Phys. Rev. B* **86**, 035132 (2012).
- [50] D. Aoki, R. Bourdarot, E. Hassinger, G. Knebel, A. Miyake, S. Raymond, V. Taufour, and J. Flouquet, Field re-entrant hidden-order phase under pressure in URu₂Si₂, *J. Phys.: Condens. Matter* **22**, 164205 (2010).
- [51] J. Buhot, M. A. Méasson, Y. Gallais, M. Cazayous, A. Sacuto, G. Lapertot, and D. Aoki, Raman scattering study of the lattice dynamic of URu₂Si₂ and sample's preparation, *J. Korean Phys. Soc.* **62**, 1427 (2013).
- [52] C. C. Homes, M. Reedyk, D. A. Crandles, and T. Timusk, Technique for measuring the reflectance of irregular, submillimeter-sized samples, *Appl. Opt.* **32**, 2976 (1993).
- [53] D. B. Tanner, Use of x-ray scattering functions in Kramers-Kronig analysis of reflectance, *Phys. Rev. B* **91**, 035123 (2015).
- [54] Z. Zhu, E. Hassinger, Z. Xu, D. Aoki, J. Flouquet, and K. Behnia, Anisotropic inelastic scattering and its interplay with superconductivity in URu₂Si₂, *Phys. Rev. B* **80**, 172501 (2009).
- [55] A. J. Millis and P. A. Lee, Large-orbital-degeneracy expansion for the lattice Anderson model, *Phys. Rev. B* **35**, 3394 (1987).
- [56] M. Scheffler, M. Dressel, M. Jourdan, and H. Adrian, Extremely slow Drude relaxation of correlated electrons, *Nature (London)* **438**, 1135 (2005).
- [57] M. Dressel and M. Scheffler, Verifying the Drude response, *Ann. Phys. (Leipzig)* **15**, 535 (2006).
- [58] P. B. Allen, Electron-phonon effects in the infrared properties of metals, *Phys. Rev. B* **3**, 305 (1971).
- [59] A. V. Puchkov, D. N. Basov, and T. Timusk, The pseudogap state in high-*T_c* superconductors: an infrared study, *J. Phys.: Condens. Matter* **8**, 10049 (1996).
- [60] D. B. Romero, C. D. Porter, D. B. Tanner, L. Forro, D. Mandrus, L. Mihaly, G. L. Carr, and G. P. Williams, Quasiparticle damping in Bi₂Sr₂CaCu₂O₈ and Bi₂Sr₂CuO₆, *Phys. Rev. Lett.* **68**, 1590 (1992).
- [61] M. Dressel and G. Grüner, *Electrodynamics of Solids: Optical Properties of Electrons in Matter* (Cambridge University Press, Cambridge, England, 2002).